Method of Determining Housing Density From Images Captured using Unmanned Aerial Vehicle (UAV)

Van B. Patiluna, Krystle Mae M. Labio, Marlowe Edgar C. Burce

Abstract —Urban density is a study in urban planning which determines the number of structures in a certain land area. The data can be interpreted in a socio-economic context such as population, income level, health risks, etc. Therefore, monitoring urban areas particularly the growth in residential areas is an important step to control the expansion and minimizing risks of epidemics, natural and man-made disasters. It also provides data to the city planners to monitor and control the urban development and provide adequate services to the populace in these areas. Remote sensing has been utilised to determine urban density by using combination of satellite images, multispectral data or combination of both. These data sources are expensive and most of the time, outdated. Therefore, an alternative platform shall be used to capture aerial images. The platform proposed are unmanned aerial vehicles (UAV). The goal of this study is to detect the density of a certain urban area using only images captured from the UAV specifically an octocopter. Since there is only one data source, an adapted workflow utilizing object-based classification method implemented in eCognition software by Definiens Imaging GmbH which is based on Fractal Net Evolution Approach (FNEA). Object-based classification is used because of higher accuracy than per-pixel classification given that only the RGB images are the available data source. The density is calculated through the ratio of structures and the land area which will be evaluated and results will be assessed in the following index range: low density, average density and high density.

Index Terms—UAV, octocopter, urban density, object-based classification.

I. INTRODUCTION

The majority of the global population today is urban. The percentage of urban dwellers increased from 43% in 1990 to 52% in 2011, and it is expected to grow to 67% by 2050 [1]. All population growth from 2011 to 2050 is expected to be absorbed by urban areas, and most of this growth will occur in cities of less developed regions [1].

Manuscript received on 27 November 2020 | Revised Manuscript received on 03 December 2020 | Manuscript Accepted on 15 December 2020 | Manuscript published on 30 December 2020.

***** Correspondence Author

Van B. Patiluna, Dept. of Computer Engineering, University of San Carlos, Cebu, Philippines,

Krystle Mae M. Labio, Dept. of Computer Engineering, University of San Carlos, Cebu, Philippines,

Dr. Marlowe Edgar C. Burce, Dept. of Computer Engineering, University of San Carlos, Cebu, Philippines,

In developing countries, rapid urban growth normally exceeds the capacity for local governments to deliver services and infrastructure, which increases urban poverty and intra-urban inequalities [2]. Urban growth leads to excessive land use as indicated by the housing density, which is the number of houses or structure in a certain land area. This expanse of urban density results in results in degradation of environmentally fragile land, occupation hazard-prone areas, loss of cultural resources, open space and excessive urban sprawl [3]. In Cebu City, Philippines heavily populated areas like slum and squatter area are estimated to be somewhere from 100,000 to 125,000 households [4]. The increase in expansion also increases risks of epidemics, natural and man-made disasters. Therefore monitoring the urban density and land use is an important step to help city planners in providing adequate resources particularly in emergency response, waste management and disaster management. Remote sensing has been utilised to determine urban density by using combination of satellite images, multispectral data or combination of both. These data sources are expensive and most of the time, outdated. Therefore, an alternative platform shall be used to capture these aerial images. UAVs are already mature enough to support the development of geoinformation products and services [5]. A particular type of UAV that is most interesting are the multi-rotors which are inexpensive and also capable of manual and automatic flight, considerable payload and acceptable range. Although limited in altitude, range and payload, this type of UAV are now widely used in scientific purposes in the field of agriculture, archaeology, biology, forestry, geology etc. Therefore, multi-rotor UAV is a sensible choice for remote sensing particularly in urban environments. It also has several advantages over conventional remote sensing platforms such as satellite and LiDaR including operational cost, flight on demand and that it could fly closer to the target area. This study demonstrates the capability of the UAV for remote sensing in urban environments. Furthermore, this study also develops a workflow in remote sensing for determining urban density using only the RGB images from the UAV.

II. MATERIALSANDMETHODS

A. Study Area

The study is conducted in one of the urban areas in Cebu City and Mandaue City in Barangay Hipodromo and Barangay Canduman. Barangay Hipodromo is adjacent to the commercial district; the Cebu Business Park and Barangay.

Canduman is located on the outskirts of the Mandaue City. The control study area was captured in Barangay Canduman, a typical urban area with houses in very close proximity with no discernible gaps in between structures.

Fig. 1. Study Area in Cebu, Philippines: Barangay Canduman in Mandaue City and Barangay Hipodromo in Cebu City (images courtesy of Google Inc.)

The area where chosen due to their representative characteristics of urban housing areas. Majority of these housing complex are on the lowlands of the city.

B. UAV as Platform for Urban Remote Sensing

UAV particularly multi-rotor systems such as an octocopter are already mature enough to support the development of geoinformation products and services. This paper will utilize UAV as a platform for urban remote sensing. Key elements in urban remote sensing using UAV are the sensor payload, flight systems, altitude, safety and noise. The development of sensors and instruments payload on UAVs is growing exponentially. This led to the increasing use of these platforms [6]. The UAV could have a payload of different imaging systems to capture high-resolution RGB and multi-spectral images. Optical sensing has advanced a lot due to the mass production of CMOS sensors widely used in consumer digital cameras and smartphones [7]. Therefore this study will focus on optical sensing using CMOS sensor from a digital camera which are less expensive than other imaging instruments. For UAVs to be successful in urban remote sensing, it has to fly higher for larger area coverage. Fixed wings systems (Fig. 2a) can fly high at a ceiling of 6000 m [8] but it should maintain a certain to maintain lift. Multi-rotors on the other hand has limited altitude but can achieve a flight ceiling of 1500 m but are cheaper to acquire and operate. Wide area coverage can be obtained by capturing mosaic of images then stitched together. To achieve this, UAVs have flight and navigational instruments as well as an electronic controller to perform flight automatically.

Fig. 2. Types of UAV used in remote sensing: a) fixed wing b) multi-rotor c) single-rotor (Images courtesy of *Headwall Photonics, **SBG Systems and ***uavgl.com)

It is therefore the conclusion of this part that UAV particularly the multi-rotor systems (Fig. 2b) are capable of the demands of urban remote sensing. This study will use a multi-rotor system to acquire orthographic images using optical sensors on a digital camera.

C. Image Acquisition

The orthographic images are captured using the octocopter UAV developed by the Center for Robotics and Automation of the University of San Carlos-Talamban Campus specifically for urban operations [9].

Fig. 3. (a) octocopter developed at the Center for Robotics and Automation, (b) actual operation

The camera used is the Canon Powershot S90 with a 6 mm focal length and a 16 megapixels CMOS sensor. To minimize image blur, a shutter speed of not lower than 1/300 s while aperture and ISO is set automatically. The camera captures a resolution of 3648 x 2736 pixels. All images are oriented to 0 degrees north. Fig. 4a shows the image captured from Barangay Canduman, Mandaue City at coordinates 10.371314, 123.933770 with the octocopter flying at an altitude of 120 m. The area represents one of the typical urban housing in Cebu. Ground resolution is approximately 28.64 pixels/meter. The houses have little or no gaps from each other. A narrow thoroughfare allows access to the housing complex. Vegetation and tree canopies are minimal in such environments. Some of the structures have long roofline that is a typical one or two floor housing building. The image in Fig. 4a will be used as the test image to calibrate and fine tune the remote sensing workflow. The image presents several variables that may affect the accuracy of the housing density. Examples of such variables are the shadows of structures cast on other structures particularly the ones on the roof and shadows on the thoroughfare and gaps between the structures. Fig. 4b shows the image captured from Barangay Hipodromo, Cebu City at coordinates 10.313518, 123.909921. This urban zone is located adjacent to the major commercial district of Cebu City, the Cebu Business Park. This sample is different from the image captured from Barangay Canduman. There are no long rooflines but the structures are more individual and heterogeneous, still there are no significant gaps between the structures.

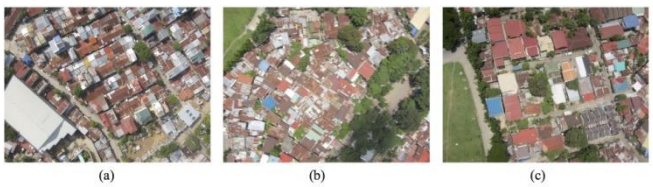

Fig. 4. (a) image from Barangay Canduman; (b) & (c) image from Barangay Hipodromo

D. Image Processing

To perform the image processing, eCognition software by Definiens AG is used in this study utilizes an object-based classification method based on Fractal Net Evolution

Approach (FNEA) technique. Object-based classification has higher accuracy than the classical per pixel method [10].

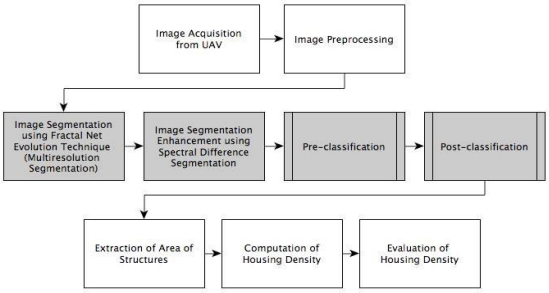

Fig. 5. System workflow

Urban indicators are extracted from the image such as vegetation, structures, shadows and asymmetric objects (roads, gaps between structures and other objects classified as otherwise). The workflow of extracting the objects is shown in Fig. 5. Other studies use several satellite image sources [11] such as SPOT5- RGB321 with multi-spectral high-resolution data, LANDSAT5 and QUICKBRD2 used for specific features of houses. However, only the orthographic RGB image will be the only source for the image processing. The pre- processing is included to make adjustments to the images acquired, which includes sharpening, noise removal, filtering etc. The image segmentation, pre-classification and post-classification were done within the domains of the eCognition software. Pre-processing is done with GIMP, an open-source image processing software.

III. THEORY/CALCULATION

A. Image Segmentation

The process of extracting the objects begins with image segmentation. Using multi-resolution segmentation or Fractal Network Evolution Approach (FNEA). A subset area was used to allow faster processing (see Fig. 6) Shape and compactness parameters are assigned both with 0.3 in multi-segmentation algorithm in eCognition. Fig. 6 shows detailed segmentation of the edges of the structures, vegetation, and roads including shadows.

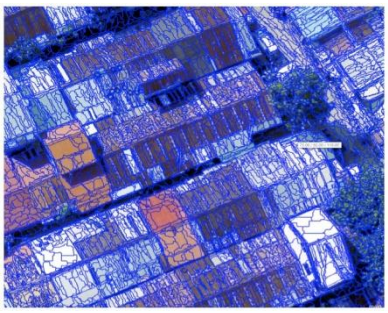

Fig. 6 Segmentation using FNEA (Segments are detailed which requires different spectral properties such as color shape and compactness)

Vegetation is classified based on spectral properties. An initial threshold condition (Mean Green Value) of >= 0.37 and second condition value (green ratio) of >= 30. Fig. 7 shows the vegetation are marked with green. Shadows are also classified by another spectral property which is its brightness. The optimal brightness threshold is <= 70 which classified shadows of structures on the roof, shadows of vegetation (tree canopy) on the ground and shadows of structures on the ground.

Fig. 7. Vegetation (green) and shadows (black) are classified (The rest are classified under surface)

Fig. 7 also details the shadows with black marks. Shadows refer to regions lacking direct solar illumination, which can be attributed to two reasons: opposing the sun and cast by obstructions [12]. As seen in Fig. 8, cast shadows from higher structures are apparent on the roofs while shadows of the structures and other objects are self-shadows.

Fig. 8. Shadows are segmented and classified as separate from the structure objects.

Shadows can provide information of the height of structures [13]-[15]. Since height of structures is not considered in this study, shadows however add another identifiable object and need to be excluded. Cast shadows on the roof shall be treated as part of the structure and not a separate object. Fig. 8 shows the cast shadows segmented by the algorithm. The next attempt to classify shadows as part of structures is done without manual classification. Additional classifications parameters are now included. Since DEM, NDSM, NIR properties are not available which could be helpful for the classification of the shadows, the parameters that involve the ratio of the red, blue and green bands are adjusted. The following parameters are applied:

*Brightness <= **70** for Shadows Mean Red = **55-189** for Structures Ratio Blue >= **0.3** and Brightness >= **70** for Structures Ratio Green >= **0.37** and Mean Green >= **30** for Vegetation*

The above parameters still include the shadows of the roof as separated from the roof, thus additional classification that involves the border in relation to a specific object is done. Additional parameters are applied:

*With border neighbor to surface >**0**pxl Relative border neighbor to vegetation <= **0.15***

In Fig. 9, the shadows from Fig. 8 are already classified as part of the roof surface.

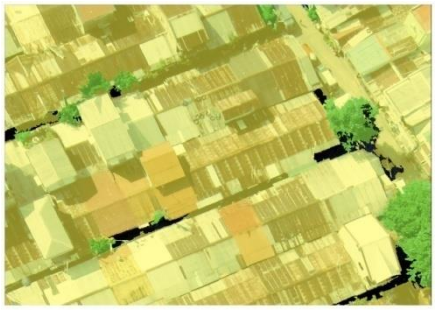

Fig. 9 Shadows classified as part of the roof.

An additional step is to convert the image objects (in pixels) to vector objects (in shapes and lines, polygons), assuming that through this type of image representation, feature extraction would be easier by using the lines or shapes generated that could have similarities and could define one roof surface from another. The next step is further looking at the usage of the vector image for feature extraction. Evaluating borders of each roof objects and grouping the borders or points together to rectangular or polygon fitting and delineate the roof objects.

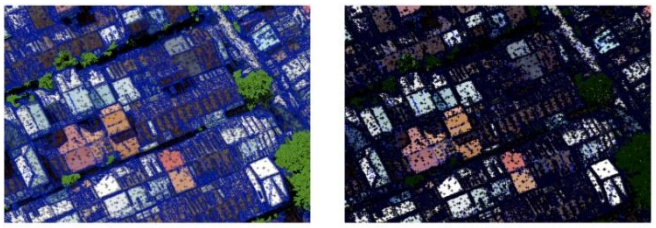

(a) (b)

Fig. 10 (a) Image converted to points and center of gravity. (b) Segmentation and classification showing the points of the vector image.

Experimenting with the values in shape = 0.3, compactness = 0.3 and scale = 10 in the segmentation parameters. Image object are converted to Points and Center of Gravity (originally polygons). The "+" marks in Fig. 10a represents the points of the polygons which are crowded in edges. This is used as basis in shape fitting to delineate the structures and shape the borders of the structures.

Fig. 10b shows the segmentation and classification showing the points of the vector image. The points are used to delineate the structures. The converted image will be stored as a thematic layer in eCognition. The structures are now represented as polygons with identifiable edges. Multi-resolution segmentation is applied at pixel level to locally minimize the average heterogeneity of the image with the given resolution. The following parameters are set in eCognition:

*Image Layer Weights: R = **1**; G = **1**; B = **1** Thematic Layer Usage = **Yes** Scale Parameter = **10** Shape = **0.3** Compactness = **0.3***

Spectral difference segmentation is applied which merges neighboring objects according to their mean layer intensity values. Maximum Spectral Difference is set to 10. Fig. 11 shows the final segmented image. The structures are classified into three (3) types, which is discussed in Section 3.C.

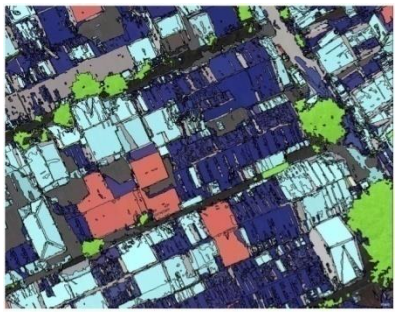

Fig. 11 Final segmented image after multi-resolution and spectral difference segmentation.

B. Object Pre-classification

This procedure divides the image based on the classification of the following objects: vegetation, structures, shadows and asymmetric objects. The table below shows the parameters set in eCognition. This allows us to exclude other objects except for the structures, which is the key indicator that is of interest of this study. Table I shows the parameters applied in eCognition for classification.

Table I.eCognition parameters for detailed classification of objects

Vegetation	Structures	Shadows	Others
Greenness Index = **2*[Green]- [Red]-[Blue]** Red = **[Mean Red]/([Mean Blue]+[Mean Green]+[Mean Red])** Green = **[Mean Green]/([Mean Blue]+[Mean Green]+[Mean Red])** Blue = **[Mean Blue]/([Mean Blue]+[Mean Green]+[Mean Red])**	*First Level Structure Classification* Mean Red value is: **50 - 190** Mean Blue value is: **50 –190** *Second Level Structure Classification (in relation to first level, based on spatial distance from neighboring objects)* Border pixels related to neighboring Structures >= **0** Border pixels related to neighboring Vegetation = **0** Relative border pixels related to neighboring Vegetation <= **0.15**	Brightness <= **60** Border pixels related to neighboring Structures >**0** Border pixels related to neighboring Vegetation >**0**	Asymmetry >= **0.9** Border pixels related to neighboring Vegetation >= **0**

All segmented objects with Greenness Index >= 0.1 are classified under Vegetation. Similar objects are merged and classified as shadows and asymmetric objects accordingly. Structures are left unmerged, as they will be classified further (see Section 3.C). Fig. 12 shows the pre-classification images generated in eCognition using the parameters in Table I.

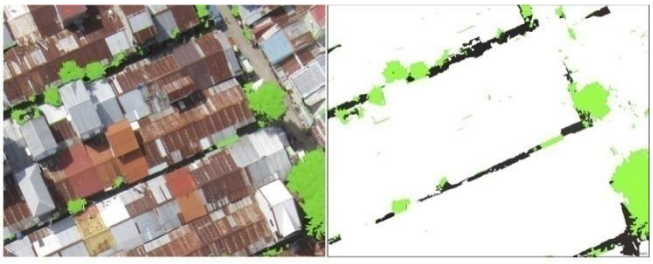

a) vegetation b) structures

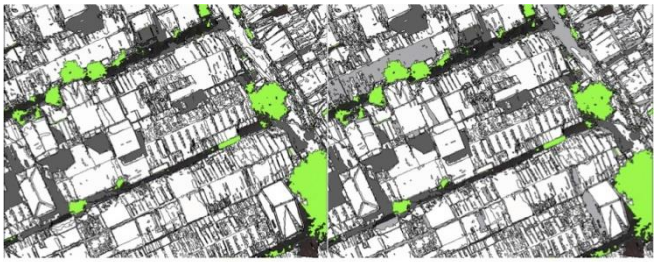

c) shadows d) asymmetric objects

Fig. 12. Pre-classification images of objects.

C. Post-classification

The post classification sub-divides the structures classified in Section 3.B. To further improve the classification derived channels calculated from original bands is applied [16]. These channels are computed as combinations of the original band or texture channels.

$$logrg = log(red) - log(green) \quad (1)$$

$$logrs = log(red) - log(red+green+blue) \quad (2)$$

Distinct color features of the roofs are identified as Light-colored (Type 1), Averagely-colored (Type 2), and Dark-colored (Type 3). Equation 1 is used to discriminate vegetation since only the green channel is subtracted while Equation 2 enhances the results of Equation 1 resulting in a more accurate classification of the structures.

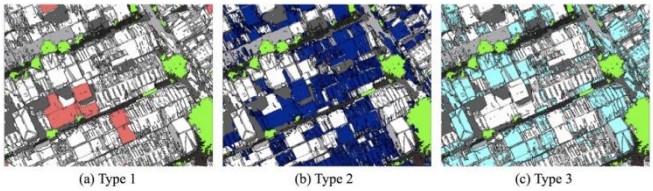

(a) Type 1 (b) Type 2 (c) Type 3

Fig. 13 Classification of roof types.

This method allows improvement of classification of structures based on the roof color and texture. It further eliminates objects, which are not considered as structures such vegetation, shadows and asymmetric objects. From Fig. 13, it is observed that applying derived channels allows deep association of objects with similar color or textures. However, there are also objects that have been identified as structures that should not be identified as such especially on Type 2 and Type 3 roof types. This will not be a problem since those objects are already identified in Section 3.B and will be disregarded during the extraction of urban features.

IV. RESULTS AND DISCUSSIONS

A. Extraction of Urban Indicators

Use The pixel areas of the detected objects from Fig. 13 are sorted and analyzed. A total of 59,601 objects detected. By manually analyzing the pixel area of an object with respect to the post-processed image (in eCognition), objects whose pixel area does not represent a structure are discarded. Fig. 14 shows the data for 900+ objects whose pixel area is above 100. Pixel areas below 9,000 are observed are erroneous objects detected especially on the texture of the roofs and other objects. Some objects detected are part of a larger object, which forms a structure.

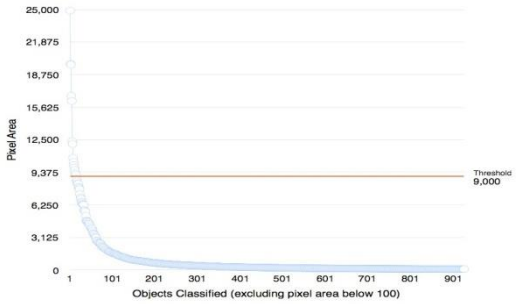

Fig. 14. Threshold of pixel area considered as structures.

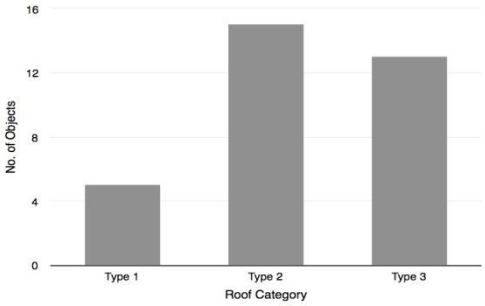

Fig. 15. No of objects per roof type

By discarding these objects, this results in a theoretical structure count of eighteen (18) structures. The manual analysis results in a structure count of thirty-three (33) leading to an error of 45.45%.

It should be noted that the automated process detected objects based on the roof characteristics. It also difficult to manually count the structures however, we counted based it on the commonality of the roof colors or texture. Since no ground data has been gathered, the manual evaluation of the structures are not accurate but will be used as baseline for the automated count. To verify whether the pixel area threshold of 9,000 if yields a lower error, the entire image captured from Barangay Canduman (see Fig. 4a) with total pixel area of 9,980,928 is subjected to the entire workflow and the number of structures are determined. The manual count for the larger area is sixty-four (64) structures while the detected number of structures is eighty-nine (89). An error of 39% is observed which is an improvement from the experiment on the subset image. Adjusting the threshold to 9,500 pixel area yields an error of only 19.42%. Images captured from Barangay Hipodromo are subjected to the workflow and the results are shown in Table II.

Table II. eCognition parameters for detailed classification of objects

Location	Pixel Area	Area (m^2)	No. of Structures (manual)	Pixel Threshold	No. of Structures (detected)	Error (%)
Canduman (subset)	1,494,108	1,821.40	33	9,000	18	45.45
Canduman (full)	9,980,928	12,170.84	64	9,000	19	39.06
Canduman (full)	9,980,928	12,170.84	64	9,500	76	18.75

Hipodromo 1	9,980,928	12,170.84	103	9,500	83	19.42
Hipodromo 2*	9,980,928	12,170.84	81	9,500	92	13.58

** Hipodromo 2 with coordinates 10.314499, 123.910117 is an image captured just north of Hipodromo 1 (see Fig. 4c). This area provides contrast to Hipodromo 1 as the structures are larger and heterogeneous in texture.*

B. Determining Density

The Philippine Statistics Authority is the central statistical authority of the Philippine government which primarily collects, compiles and analyzes data on the different sectors of the economy. Although the agency collects data on population density (number of persons per km^2), there are no documented metrics on urban housing density. Determining the urban housing density will be approached with the following indices: number of structures and the area of the land of a given jurisdiction. In this study, density is measured by the following: *density_alpha = number of structures/total land area* (3) *density_beta = number of structures/2500 m^2*(4)

Equation (3) calculates the number of structures in a given jurisdiction such as the entire area of a barangay, which does not limit to dwellings. Another indicator is the number of structures in a 2,500 m^2 land area as shown in (4). A 2,500 m^2 sample was taken from the image which only consist mainly of structures, then the number of structures are counted.

Table III. Determining the housing density.

Location	Area (m^2)	Structures (detected)	density alpha	density beta
Canduman (full)	12,170.84	76	0.0062	0.0128
Hipodromo 1	12,170.84	83	0.0068	0.0100
Hipodromo 2	12,170.84	92	0.0076	0.016

To classify the density computed, the data from the demographic and socio-economic profile of Cebu [17] are used as basis. Data of floor area of the houses in Cebu City and Mandaue City are classified as shown in Fig. 16.

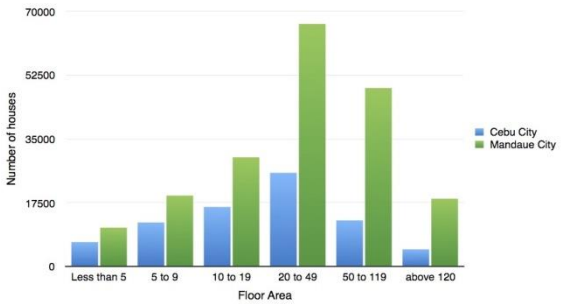

Fig. 16. Classification of floor area of houses in Cebu City and Mandaue City.

Majority of the houses are in the 20 to 49 m^2 range, which includes the typical middle class houses. This data will be used as the basis of the density classification, which is shown in Table IV. The proposed density classification is based on the floor area category and the possible number of houses in a 2,500 m^2 land area. The upper class of High Density is based on the median floor area from 1 to 49 where most of these floor areas are in the urban part of the city. The lower class considers the range of 40 to 80 houses with an area of 62.5 m^2. With decreasing floor area, the number of houses also increases. The Average Density has a range from 21 to 39 also taking into account the direct relationship of the floor area and the number of houses; while Low Density is calculated starting from houses with an area of 120 m^2 based on the last classification of floor area in Fig. 16.

Table IV. Density classification per 2,500 m^2.

Classification	No. of houses per m^2
High Density	> 80
	40 to 80
Average Density	21 to 39
Low Density	< 21

Applying the density classification on the three images from Barangay Canduman and Barangay Hipodromo results in the density classification in Table V. It is noted that the images are only subset of the entire barangay.

Table V. Density classification of the sample images.

Location	No. of houses per m^2	density_beta	Density Classification
Canduman (full)	32	0.0128	Average
Hipodromo 1	42	0.0168	High
Hipodromo 2	25	0.0100	Average

It is also worth noting that the density_alpha values corresponds to the density_beta except for Hipodromo 1 due to the fact that the workflow detected more structures in Hipodromo 2. By manual analysis, Hipodromo 1 is the most dense with structures compacted together in a small area. Canduman is second while Hipodromo 2 is obviously less dense.

ACKNOWLEDGMENT

The authors would like to acknowledge the Office of Population Studies at the University of San Carlos for providing the data on the barangays in Cebu City and Mandaue City. Special thanks also to the Barangay Councils of Canduman and Hipodromo for allowing us to capture aerial photographs on their jurisdictions.

REFERENCES

1. GUnited Nations World Urbanization Prospects, the 2012 Revision,
2. 2012. Retrieved July 20, 2016, from http:// www.un.org/en/development/desa/publications/world-population-prospects-the-2012-revision.html.
3. J. Duque, J. Patino, L. Ruiz, J. Pardo-Pascual, "Measuring intra-urban poverty using land cover and texture metrics derived from remote sensing data," Landscape and Urban Planning vol. 135, Nov. 2014, 135, pp. 11-21.
4. J. Bernstein, "Land use considerations in urban environmental management,"1994. Retrieved July 20, 2016, from http://elibrary.worldbank.org/doi/abs/10.1596/0-8213-2723-2#.
5. Kobe International Community Center Report Section G. Cebu City, Philippines. Retrieved July 25, 2016, from http://www.kicc.jp/auick/database/ids/ids02/Cebu.pdf.
6. I. Colomina& P. Molina, "Unmanned aerial systems for photogrammetry and remote sensing: A review," ISPRS Journal of Photogrammetry and Remote Sensing vol. 92, April 2014, pp. 79-97.

7. G. Pajares, “Overview and Current Status of Remote Sensing Applications Based on Unmanned Aerial Vehicles (UAVs),” Photogrammetric Engineering & Remote Sensing vol. 81, April 2015, pp. 281-329.
8. C. Toth & G. Jóźków, “Remote sensing platforms and sensors: A survey,” ISPRS Journal of Photogrammetry and Remote Sensing vol.
9. 115, May 2016, pp. 22-36.
10. X. Tianyun, T. Xiaocheng, Y. Defang, X. Yonghe, & Y. Hongliang, “UAV Remote Sensing Applications in Large-scale Mapping in the Hilly Region of Tibetan Plateau,” International Journal of Control and Automation vol. 3, 2015(3), pp. 279-286.
11. V. Patiluna& M.E. Burce, “Unmanned Aerial Vehicle for Urban Remote Sensing,” *IECEP Journal*, submitted for publication.
12. S. Myint, P. Gober, A. Brazel, S. Grossman-Clarke, & W. Qihao, “Per-pixel vs object-based classification of urban land cover extraction using high spatial resolution imagery,” Remote Sensing of Environment vol. 115, 2010, pp. 1145-1161.
13. S. d’Oleire-Oltmans, B. Coenradie, & B. Kleinscheit, “An object-based classification approach for Mapping Migrant Housing in the Mega-Urban Area of the Pear River Delta,” Remote Sensing vol.
14. 3, 2011, pp. 1710-172.
15. H. Li, L. Xuc, H. Shena, & L. Zhangd, “A general variational framework considering cast shadows for the topographic correction of remote sensing imagery,” ISPRS Journal of Photogrammetry and Remote Sensing vol. 117, July 2016, pp. 161-171.
16. K.R.M. Adeline, M. Chen, X. Briottet, S.K. Pang, & N. Paparoditis, “Shadow detection in very high spatial resolution aerial images: A comparative study,” ISPRS Journal of Photogrammetry and Remote Sensing vol. 80, June 2013, pp. 21– 38.
17. N. Al-Najdawi, H.E. Bez, J. Singhai, & E.A. Edirisinghe, “A survey of cast shadow detection algorithms,” Pattern Recognition Letters vol.
18. 33, 2012, pp. 752–764.
19. F. Cheng & F.H. Thiel, “Delimiting the building heights in a city from the shadow in a panchromatic SPOT- image. Part 1. Test of forty-two buildings,” International Journal of Remote Sensing, vol. 16, 1995, pp. 409–415.
20. A. Le Bris & P. Robert-Sainte, “Classification of Roof Materials for
21. Rainwater Pollution Modelization,” ISPS Proceedings vol. 28, 2012, Retrieved September 5, 2106, from http://www.isprs.org/proceedings/XXXVIII/1_4_7-W5/paper/ LE_BRIS-152.pdf.
22. S. Gultiano& D. Xenos, “Cebu: A Demographic and Socio-economic Profile based on the 2010 Census,” USC Press, 2015.